ELSEVIER

Nuclear Instruments and Methods in Physics Research B 179 (2001) 343–350

NIM B
Beam Interactions with Materials & Atoms

www.elsevier.com/locate/nimb

Experimental and theoretical features of hard-collimated type-B coherent high energy pair production

I. Endo [a], Y. Okazaki [b], Yu.P. Kunashenko [c], Yu.L. Pivovarov [c,*]

[a] *Graduate School of Advanced Sciences of Matter, Hiroshima University, Higashi-Hiroshima 739-8526, Japan*
[b] *Faculty of Science, Hiroshima University, Higashi-Hiroshima 739-8526, Japan*
[c] *Nuclear Physics Institute, Tomsk Polytechnic University, 634050 Tomsk, Russia*

Received 28 April 2000; received in revised form 5 December 2000

Abstract

We have reexamined the conditions for the enhancement of electron–positron pair photoproduction cross-section to occur due to the type-B coherent effect. Simple formulae to characterize the position and the bandwidth of the enhancement for the hard collimated pairs are derived. We also examined the effect of interference among the atomic strings and found that, in some cases it is almost identical to a random phase approximation while in other cases, phenomena analogous to the extinction law in X-ray diffraction may occur.

PACS: 12.20.-m; 61.80.Fe

1. Introduction

When a high-energy photon enters a crystal in parallel to its crystallographic axis, a sharp rise in e^+e^- pair production cross-section is expected to occur at a photon energy where the longitudinal component of the momentum transfer $\boldsymbol{q}$ coincides with integer multiples of h/d, where h and d are the Planck constant and the crystallographic plane spacing, respectively [1]. This phenomenon is known as type-B coherent pair production and has been observed by several experiments [2–4]. The most recent experiment [4], in particular, has demonstrated the clearest evidence of the enhancement making use of the fact that the more prominent enhancement is expected if we restrict ourselves to observe the pairs emitted at small angles [5]. The existing theoretical works evaluated the coherent effect based on the one-dimensional (1-D) model: the enhancement of cross-section occurs due to the coherent sum of production amplitude from periodically spaced atoms along a crystal axis, while the observable cross-section from a bulk of crystal is obtained by an incoherent sum of strings. However, the actual crystal has periodic structure in the three-dimensional (3-D) space and it is necessary to consider the

* Corresponding author.
E-mail address: pivovarov@fnsm.tpu.edu.ru (Y.L. Pivovarov).

0168-583X/01/$ - see front matter
PII: S0168-583X(00)00692-3

interference between strings and the substructures along a crystal axis. The purpose of the present work is to reconsider the conditions under which the enhancement due to type-B coherent effect is observable and then to discuss the predicted features to be experimentally verified.

2. Kinematical consideration

The momentum transfer $\boldsymbol{q}$ in the pair production process is defined by

$$\boldsymbol{q} = \boldsymbol{k} - \boldsymbol{p}_+ - \boldsymbol{p}_-, \tag{1}$$

where $\boldsymbol{k}$, $\boldsymbol{p}_+$ and $\boldsymbol{p}_-$ denote momenta of the incident photon and the created positron and electron, respectively. Hereafter, we use a unit in which the light velocity c is unity, i.e., $c = 1$. According to the 1-D model of type-B coherent pair production where the atoms are equally spaced along a crystal axis by the relative position $\boldsymbol{d}$ ($|\boldsymbol{d}| = d$) the longitudinal component of momentum transfer defined by $q_\parallel = \boldsymbol{q} \cdot \boldsymbol{d}/d$ determines the condition for the enhancement to occur:

$$q_\parallel = nh/d = \ell_n, \tag{2}$$

for any integer n. Making use of energy conservation

$$\omega = E_+ + E_-, \tag{3}$$

where $\omega = k$ is the incident photon energy while $E_- = \sqrt{p_-^2 + m_e^2}$ ($E_+ = \sqrt{p_+^2 + m_e^2}$) is the electron (positron) energy with m_e being the electron mass, we can calculate $q_\parallel$. At small emission angles and high energies, $E_\pm^2 \gg m_e^2$, it is approximated by a simple expression as

$$q_\parallel = \frac{A}{\omega} + B\omega, \tag{4}$$

$$A = \frac{m_e^2}{2x_+(1-x_+)}, \tag{5}$$

$$B = \frac{\theta_+^2 x_+}{2} + \frac{\theta_-^2(1-x_+)}{2}, \tag{6}$$

where θ_- (θ_+) denotes the polar angle of emitted electron (positron) and x_+ stands for the fractional positron energy $x_+ = E_+/\omega$, and $x_+ + x_- = 1$. For fixed emission angles, this gives a parabolic curve as depicted in Fig. 1. The condition for the nth-order enhancement (2) is satisfied at both

$$\omega_n(\theta_+, \theta_-) = \frac{\ell_n - \sqrt{\ell_n^2 - 4AB}}{2B} \tag{7}$$

and

$$\omega_n'(\theta_+, \theta_-) = \frac{\ell_n + \sqrt{\ell_n^2 - 4AB}}{2B} \tag{8}$$

under the condition that $\ell_n^2 \geqslant 4AB$ and $B \neq 0$. For zero emission angles ($B = 0$), it reduces to

$$\omega_n(0,0) = \frac{m_e^2}{2x_+(1-x_+)}\frac{d}{nh}. \tag{9}$$

It is interesting to note that there are two possible solutions, $\omega_n(\theta_+, \theta_-)$ and $\omega_n'(\theta_+, \theta_-)$, for non-zero emission angles for which no attention has been paid before, although this is completely trivial.

In a practical case, the emission angles are not exactly specified but are allowed to be in the region between zero and a certain maximum angle θ_{max}. Therefore, the expected nth order peak, for fixed x_+, shows up as an enhanced energy region with a bandwidth

$$\Delta\omega_n = \omega_n(\theta_{max}, \theta_{max}) - \omega_n(0,0). \tag{10}$$

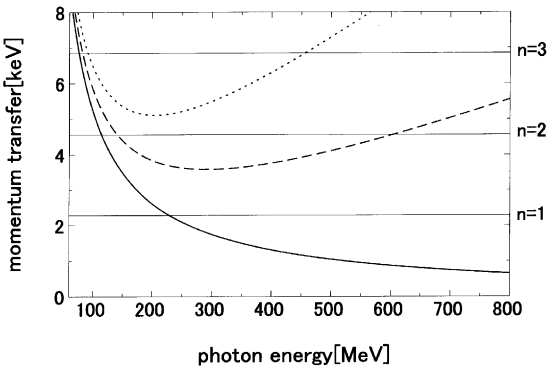

Fig. 1. The longitudinal momentum transfer q_ℓ for symmetric pair production is shown as a function of photon energy ω. The solid, dashed and dotted lines correspond to the emission angles of 0, 3.5 and 5.0 mrad, respectively. The horizontal lines are to show the condition of $q_\parallel$ to satisfy the first-, second- and third-order enhancements for Si⟨100⟩ axial orientation.

For small $\theta_{\max}$ it can be approximated as

$$\Delta\omega_n = \omega_n^3(0,0)\frac{x_+(1-x_+)}{m^2}\theta_{\max}^2. \tag{11}$$

The x_+ dependence of coherent peak is also easily obtained from Eq. (9). The relative shift of threshold energy with respect to $\omega_n(0,0)$ for symmetric pairs $(x_+ = 0.5)$ is found to be $[1/4x_+(1-x_+)-1]$ and is shown in Fig. 2.

The higher energy solution for small emission angles is obtained from (8) such that

$$\omega_n'(\theta_+,\theta_-) = \frac{2\ell_n}{\theta_+^2 x_+ + \theta_-^2(1-x_+)} - \frac{m_e^2}{x_+(1-x_+)\ell_n}. \tag{12}$$

This means that the enhancement of collimated pairs corresponding to the higher energy solution looks like a stepwise rise at $\omega_n'(\theta_{\max},\theta_{\max})$ followed by a slowly varying plateau up to the highest possible energy, because $\omega_n'(\theta_+,\theta_-)$ increases as the emission angles decrease from $\theta_{\max}$.

3. Interference between strings (3-D model)

The atomic strings in actual crystals are not random but are periodically separated from each other, say, by $\boldsymbol{s}$. The amplitude of pair creation from all the strings is then expressed by a sum of the contribution from each string multiplied by a phase factor $\exp(i\boldsymbol{q}\cdot\boldsymbol{s})$. (In this section the momentum transfer $\boldsymbol{q}$ is measured in units $\hbar$.) This procedure is, by changing the order of summation, shown to be equivalent to a well-known 3-D model used to evaluate the coherent bremsstrahlung [6].

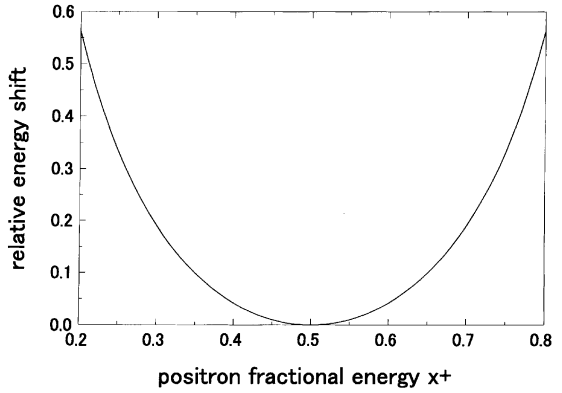

Fig. 2. The relative shift of threshold energy of coherent peak for asymmetric pairs with respect to the symmetric ones is shown as a function of fractional positron energy x_+.

When we detect the pairs with emission lesser than $\theta_{\max}$, the enhancement of cross-section comes from the integration of coherent cross-section,

$$\frac{d\sigma_{\rm coh}}{dx_+} = \int_0^{\theta_{\max}}\int_0^{\theta_{\max}}\int_0^{2\pi}\frac{d\sigma_{\rm coh}}{dx_+ d\theta_+ d\theta_- d\phi_+}d\theta_+ d\theta_- d\phi_+, \tag{13}$$

where the angular variable ϕ_+ stands for the azimuthal angle of the positron relative to the electron azimuthal angle. Following the standard prescription, this integration is expressed by the sum of contribution from the reciprocal lattice points using the single atom cross-section $d\sigma_1$ ($d\sigma_1$ is a single atom cross-section of the pair creation, e.g. the Bethe–Heitler–Born approximation cross-section taking into account the screening effect),

$$\frac{d\sigma_{\rm coh}}{dx_+} = C\sum_{l,m,n}\frac{d\sigma_1}{dx_+ dq_x dq_y dq_z}\exp(-q_{lmn}^2\bar{u}^2)|S(\boldsymbol{q}_{lmn})|^2, \tag{14}$$

where C is a conversion factor used in approximating the Laue function with the delta function in

$$\delta(q_x - lb_x)\delta(q_y - mb_y)\delta(q_z - nb_z),$$

with b_x, b_y, b_z being the spacing in the reciprocal lattice points, $\boldsymbol{q}_{hkl}$ is the momentum transfer on the reciprocal lattice points specified by the Miller index $(lmn) : (q_x = lb_x,\ q_y = mb_y,\ q_z = nb_z)$. The thermal vibration of the crystal lattice is taken into account by the Debye–Waller factor $\exp(-q^2\bar{u}^2)$, where $\bar{u}^2$ is the mean-square value of the thermal vibration amplitude of the atom depending on the crystal temperature T ($\bar{u}^2 = \bar{u}^2(T)$). The factor $|S(\boldsymbol{q}_{lmn})|^2$ comes from the contribution of partial sum within the unit cell giving rise to a sum of phase factors, called the structure factor,

$$S(\boldsymbol{q}) = \sum_{j=1}^{N} \exp(\mathrm{i}\boldsymbol{q} \cdot \boldsymbol{r}_j), \tag{15}$$

where $\boldsymbol{r}_j$ is the position of the jth atom in the unit cell containing N atoms. Generally speaking, these N atoms belong to different atomic strings, and therefore $S(\boldsymbol{q}_{lmn})$ describes the interference between crystal strings. It is to be emphasized that the cross-section is proportional to $|S(\boldsymbol{q}_{lmn})|^2$ which takes a value between 0 and N^2 depending upon both the crystal structure and the momentum transfer. The condition that we detect the collimated pairs is imposed by specifying the allowed reciprocal lattice points in the summation (14) to be consistent with the allowed angular region, $\theta_{\pm} < \theta_{\max}$.

4. Interference effects for diamond-like crystals in 3-D model

As is well known, the structure factor for a diamond-like crystal at the reciprocal lattice point specified by the Miller indices h, k, l is written as follows:

$$\begin{aligned} |S|^2 &= 64 \quad \text{for } l,m,n \text{ even and} \\ &\qquad l+m+n \text{ is multiples of 4;} \\ &= 32 \quad \text{for all of } l,m,n \text{ are odd;} \\ &= 0 \quad \text{neither of the above.} \end{aligned} \tag{16}$$

Now let us take a coordinate system fixed to the crystal axis such that l, m, n corresponds to the x, y, z direction, respectively. In the case that the photon beam is parallel to the z-axis, the nth order type-B coherent peak is a sum of contribution from the reciprocal points on the plane $z = nb_z$, where b_z represents the spacing of lattice points in the z direction. Each point has a weight factor proportional to Eq. (16) depending on l. In Fig. 3 we show the structure factors on the reciprocal lattice plane corresponding to $n = 1$, 2, 3 and 4. The horizontal lines show the intersections of a constant-n plane with the constant-l planes, while the vertical lines are for those with constant m. The crossing points correspond to the various combination of (l,m) with n fixed to the value attached

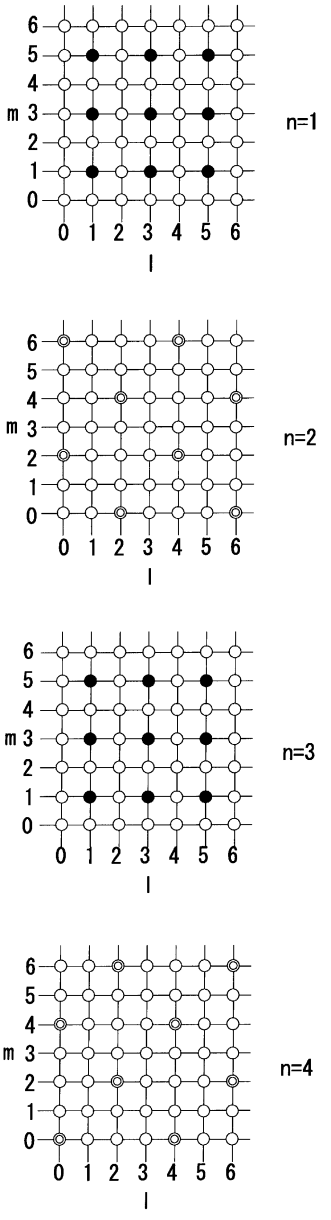

Fig. 3. The structure factors relevant to the Si ⟨100⟩ type-B effect is demonstrated. The horizontal lines show the intersections of a constant-n plane with the constant-l planes, while the vertical lines are for those with constant m. The crossing points correspond to the various combination of (l,m) with n fixed to the value attached at the right-hand side of the figures. From the top to the bottom, the structure factors $|S|^2$ at the reciprocal lattice plane responsible for the $n = 1$, 2, 3, 4 peaks are shown. The double circles, closed circles and open circles represent the points with $|S|^2$ being 64, 32 and 0, respectively.

at the right-hand side of the figures. The double, closed and open circles represent the reciprocal lattice points with $|S|^2$ equal to 64, 32 and 0, respectively.

In the case that the photon enters parallel to the direction $\langle 1\,1\,1\rangle$, the plane perpendicular to the beam direction is expressed by $l+m+n=n'$. The horizontal lines show the intersections of a constant-n' plane with the constant-l planes, while the slant lines from up-left (up-right) to down-right (down-left) are for those with constant $m(n)$. The crossing points correspond to the various combinations of (l,m,n) with n' fixed to the value attached at the right-hand side of the figures. The structure factors on the $n'=1$, 2, 3, 4 planes are shown in Fig. 4 in the same manner as in Fig. 3.

5. Interference within a string in 1-D model

Although the atoms are equally spaced by d along a straight line in a naive 1-D model, there are cases where several atoms exist within an interval d. Let us call the minimum unit of periodic structure as the "unit segment". The contribution of atoms within the unit segment to the pair creation amplitude should be summed up as in (15). Denoting the distance of the jth atomic position from the origin of the unit segment as r_j, we obtain the "string–structure factor" as

$$S_{\mathrm{s}}(q_{\parallel})=\sum_{j=1}^{N}\exp(\mathrm{i}q_{\parallel}r_j), \tag{17}$$

where N is the number of atoms in the unit segment.

6. Experimental features for $\langle 1\,0\,0\rangle$ and $\langle 1\,1\,1\rangle$ Si crystal

In a practical experiment the momentum vectors of the emitted e^+ and e^- are allowed to point any direction within a predefined maximum angle $\theta_{\max}$. Thus the observed lth enhancement in cross-section is the sum of contributions of reciprocal lattice points in a plane perpendicular to the beam axis at $q_{\parallel}=lh/d$. In the experiment of [4], for example, the allowed angular region of emitted pairs is defined by an active collimator so that the maximum transverse momentum was 0.23 MeV for 2-mrad collimation. The spacing of the recip-

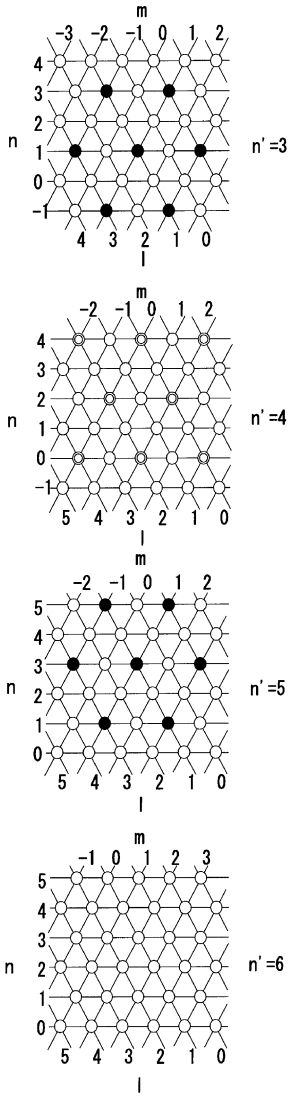

Fig. 4. The structure factors relevant to the Si $\langle 1\,1\,1\rangle$ type-B effect is demonstrated. The horizontal lines show the intersections of a constant-$n'=(l+m+n)$ plane with the constant-l planes, while the slant lines from up-left (up-right) to down-right (down-left) are for those with constant $m(n)$. The crossing points correspond to the various combination of (l,m,n) with n' fixed to the value attached at the right-hand side of the figures. The double circles, closed circles and open circles represent the points with $|S|^2$ being 64, 32 and 0, respectively.

rocal lattice is 2.2877 keV for Si so that the experiment accepts the contribution from as many as about 600 reciprocal lattice points. This is approximately equivalent to the integration over the transverse momentum as in 1-D model with the average value of $|S|^2$, denoted by $\overline{|S|^2}$, which is dependent on the crystal structure and the choice of crystallographic axis. For Si $\langle 1\,0\,0\rangle$, $\overline{|S|^2}$ is easily obtained by inspecting Fig. 3: for $n=1$, each double circle is accompanied by seven open circles making $\overline{|S|^2}=(64+7\times 0)/8=8$. For $n=2$, we come to the same mean value again, because a solid circle is accompanied by three open circles making $\overline{|S|^2}=(32+3\times 0)/4=8$. In this way we can prove that $\overline{|S|^2}=8$ for any n for $\langle 1\,0\,0\rangle$ Si crystal. As the unit cell of Si crystal is made of eight atoms, the average contribution from a reciprocal lattice point is identical to the incoherent sum of contribution of atoms in the unit cell. Therefore the 1-D model is a good approximation to the problem. For Si $\langle 1\,1\,1\rangle$ axis, however, we found

$$\begin{aligned}\overline{|S|^2} &= 8 \quad \text{for } n'=1,3,5,\ldots,\\ &= 16 \quad \text{for } n'=4,8,12,\ldots,\\ &= 0 \quad \text{for } n'=2,6,10,\ldots,\end{aligned} \tag{18}$$

where the integer

$$n'=l+m+n \tag{19}$$

is the order of coherent peak.

In Fig. 5 we show, as an example, a pattern of expected type-B coherent peaks for the pair production from $\langle 1\,1\,1\rangle$ Si crystal with the bremsstrahlung from a 150 MeV electron ring REFER at Hiroshima University. The collimation angle of emitted pairs is assumed to be 3.5 mrad. The calculation is made for the crystal temperature $T=293$ K. The vertical axis indicates the sum of coherent and incoherent cross-section normalized by the cross-section of amorphous target. As one can see from Fig. 5, the amount of enhancement is large due to the collimation effect predicted in [5].

The 1-D model for this case gives a structure factor coming from the two atomic positions in the unit segment: one at the origin and the other at one-fourth of the unit segment length. From (17),

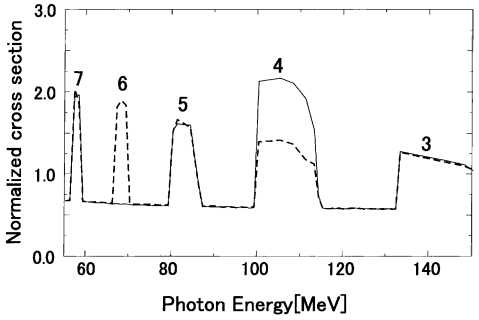

Fig. 5. Predicted feature of type-B coherent peaks from $\langle 1\,1\,1\rangle$ Si crystal expected with the bremsstrahlung from 150 Mev electron ring REFER ($x_+=0.5$). The vertical axis represents the sum of coherent and incoherent cross-section normalized by the cross-section on an amorphous target. The collimation angle of emitted pairs is assumed to be 3.5 mrad, the crystal temperature $T=293$ K. The solid curve corresponds to the case where the interference effect in the unit cell or unit segment for 3-D and 1-D models, respectively, is taken into account. For comparison, a fictitious case where such interference is neglected is shown by the dashed line. The particular angle 3.5 mrad is chosen for expected real experimental conditions at REFER.

we obtain the squared structure factor that becomes

$$|S_s(l')|^2=4\cos^2\left(\frac{l'\pi}{4}\right),\quad l'=1,2,3,\ldots. \tag{20}$$

Quite surprisingly, the structure factor of 1-D model is identical to the averaged structure factor in 3-D model (18) if we normalize them by the number of atoms in the substructure,

$$W=\overline{|S(n')|^2}/8=|S_s(n')|^2/2. \tag{21}$$

Thus the predictions with the 1-D and 3-D models are almost the same provided the relevant number of reciprocal lattice points are large enough to take an average.

The conditions for the peaks to appear are summarized in Tables 1 and 2 for Si$\langle 1\,0\,0\rangle$ and Si$\langle 1\,1\,1\rangle$, respectively. Note that the last columns show the weight factor W due to the interference effect. As an example we show an expected energy dependence of pair production from a Si$\langle 1\,1\,1\rangle$ target from 150 MeV bremsstrahlung at REFER facility in Hiroshima. It is normalized by the expected cross-section for an amorphous target. The

Table 1
Expected photon energies, in MeV, of coherent peaks for Si $\langle 1\,0\,0\rangle$ are shown[a]

θ	0 mrad	1.0 mrad		3.5 mrad		
n	ω	ω	ω'	ω	ω'	$\overline{\lvert S\rvert^2}/8$
1	228.25	240.94	4334.96	–	–	1
2	114.13	115.58	9036.22	140.58	606.50	1
3	76.09	76.51	13651.21	82.10	1038.53	1
4	57.06	57.24	18246.38	59.42	1434.74	1
5	45.65	45.74	22833.79	46.82	1820.89	1
6	38.04	38.09	27417.34	38.71	2202.54	1
7	32.61	32.64	31998.71	33.02	2581.77	1

[a] The first column refers to the order of enhancement. ω and ω' are low energy and high energy solutions found in Eqs. (7) and (8). The emission angles of both electrons and positrons are specified to be θ appearing in the top row. The last column indicates the weight factor mentioned in the beginning of Section 6.

Table 2
Expected photon energies, in MeV, of coherent peaks for Si$\langle 1\,1\,1\rangle$ are shown[a]

θ	0 mrad	1.0 mrad		3.5 mrad		
n'	ω	ω	ω'	ω	ω'	$\overline{\lvert S\rvert^2}/8$
1	395.35	484.03	2157.86	–	–	1
2	197.68	205.68	5078.12	–	–	0
3	131.78	134.05	7791.65	184.25	462.73	1
4	98.83	99.78	10467.82	113.86	748.79	2
5	79.07	79.54	13129.95	85.91	992.41	1
6	65.89	66.16	15785.24	69.63	1224.35	0
7	56.48	56.65	18436.65	58.76	1450.89	1

[a] See the caption of Table 1 for the explanation of symbols. The last column indicates the weight factor mentioned in Eq. (18).

collimation angle $\theta_{\max}$ is taken to be 3.5 mrad. While the dashed curve indicates a fictitious case where the interference within the substructure is neglected, the solid curve takes into account the interference in 3-D or 1-D substructure by the structure factor (18) or (20), respectively. Small difference in numerical values obtained in 1-D and 3-D calculations is neglected here. Here we see the $n' = 4$ peak is twice as high as the noninterference case while the sixth peak disappears due to the extinction law.

7. Conclusion

Inspired by recent experimental works on type-B coherent pair photoproduction, we have reexamined the condition under which the cross-section enhancement is observable. We have found the following:

1. For fixed emission angles, there are two possible solutions in photon energy, referred to as the higher and the lower energy solutions, for the coherent enhancement to occur.
2. The collimation angle of emitted pairs defines the bandwidth of the coherent peak corresponding to the lower energy solution.
3. Due to the interference effect among the contributions from the substructures in a unit cell in 3-D model (a unit segment in 1-D model), structure factors analogous to those for the X-ray diffraction show up.
4. For the $\langle 1\,1\,1\rangle$ direction of diamond-like crystals, both 1-D and 3-D models predict almost

identical feature in the energy dependence of the cross-section: some peaks disappear and others have larger enhancement factor due to the interference.

The existing experimental data are insufficient to verify these features and further precision experiments are desirable.

Acknowledgements

This work was supported by Grant-in-aid for Scientific Researches Monbusho No. 08404016, by Grant from Russian Education Ministry No. 97-06.2-40 and by Grant from Russian State Program "Fundamental Nuclear Physics", Project 135-09.

References

[1] N. Cue, J.C. Kimball, Phys. Lett. A 124 (1987) 191.
[2] R.O. Avakyan, A.E. Avetisyan, V.A. Gyurdzhyan, K.R. Dallakyan, S.S. Danagulyan, S.M. Darbiriyan, K.A. Ispiryan, O.S. Kizogyan, A.T. Margaryan, Yu.Z. Sukiasyan, S.P. Taroyan, Pis'ma Zh. Eksp. Teor. Fiz. 51 (1990) 627 [JETP Lett. 51 (1990) 396].
[3] M.Yu. Andreyashkin, A.Yu. Basai, S.A. Vorobiev, V.N. Zabaev, B.N. Kalinin, Yu.P. Kunashenko, Yu.L. Pivovarov, Pis'ma Zh. Eksp. Teor. Fiz. 55 (1992) 407 [JETP Lett. 55 (1992) 413].
[4] Y. Okazaki, M. Andreyashkin, K. Chouffani, I. Endo, Y. Hasegawa, M. Iinuma, S. Nakagawa, T. Ohnishi, T. Takahashi, R. Hamatsu, H. Kojima, M. Masuyama, H. Okuno, Y. Takashima, Yu.P. Kunashenko, Yu.L. Pivovarov, Phys. Lett. A 271 (2000) 110.
[5] Yu.P. Kunashenko, Yu.L. Pivovarov, Nucl. Instr. and Meth. B 114 (1996) 237.
[6] G. Diambrini-Palazzi, Rev. Mod. Phys. 40 (1968) 611.